# One- and two-band models for colossal magnetoresistive manganites studied using the truncated polynomial expansion method

C. Şen,[1] G. Alvarez,[2] Y. Motome,[3] N. Furukawa,[4] I. A. Sergienko,[5,6] T. C. Schulthess,[2] A. Moreo,[5,6] and E. Dagotto[5,6]
[1]*National High Magnetic Field Laboratory and Department of Physics, Florida State University, Tallahassee, Florida 32310, USA*
[2]*Computer Science & Mathematics Division, Oak Ridge National Laboratory, Oak Ridge, Tennessee 37831, USA*
[3]*RIKEN (The Institute of Physical and Chemical Research), Saitama 351-0198, Japan*
[4]*Department of Physics and Mathematics, Aoyama Gakuin University, Sagamihara 229-8558, Japan*
[5]*Condensed Matter Sciences Division, Oak Ridge National Laboratory, Oak Ridge, Tennessee 32831, USA*
[6]*Department of Physics and Astronomy, The University of Tennessee, Knoxville, Tennessee 37996, USA*
(Received 25 August 2005; revised manuscript received 24 April 2006; published 23 June 2006)

Considerable progress has been recently made in the theoretical understanding of the colossal magnetoresistance (CMR) effect in manganites. The existence of inhomogeneous states has been shown to be directly related with this phenomenon, both in theoretical studies and experimental investigations. The analysis of simple models with two competing states and a resistor network approximation to calculate conductances has confirmed that CMR effects can be theoretically reproduced using nonuniform clustered states. However, a direct computational study of the CMR effect in realistic models has been difficult since large clusters are needed for this purpose. In this paper, the recently proposed truncated polynomial expansion method (TPEM) for spin-fermion systems is tested using the double-exchange one-orbital, with finite Hund coupling $J_H$, and two-orbital, with infinite $J_H$, models. Two dimensional lattices as large as $48\times48$ are studied, far larger than those that can be handled with standard exact diagonalization (DIAG) techniques for the fermionic sector. The clean limit (i.e., without quenched disorder) is analyzed here in detail. Phase diagrams are obtained, showing first-order transitions separating ferromagnetic metallic from insulating states. A huge magnetoresistance is found at low temperatures by including small magnetic fields, in excellent agreement with experiments. However, at temperatures above the Curie transition the effect is much smaller confirming that the standard finite-temperature CMR phenomenon cannot be understood using homogeneous states. By comparing results between the two methods, TPEM and DIAG, on small lattices, and by analyzing the systematic behavior with increasing cluster sizes, it is concluded that the TPEM is accurate enough to handle realistic manganite models on large systems. Our results contribute to the next challenge in theoretical studies of manganites, namely a frontal computational attack of the colossal magnetoresistance phenomenon using double-exchange-like models, on large clusters, and including quenched disorder.

DOI: 10.1103/PhysRevB.73.224430 PACS number(s): 75.47.Lx, 75.30.Mb, 75.30.Kz

## I. INTRODUCTION

The study of transition metal oxides (TMOs) has been among the most important areas of investigations in condensed matter physics in the last two decades. The excitement in this context started with the high-temperature superconductors and was later followed by the discovery of the colossal magnetoresistance in manganites,[1–8] as well as a plethora of equally interesting phenomena in several other oxides. Strong correlations (i.e., large electron-electron or electron-phonon couplings, or both) play a major role in the physics of these materials. In addition, the presence of nearly degenerate states renders some of these oxides highly susceptible to external perturbations. In fact, TMOs appear to share a phenomenology similar to that of complex systems, with nonlinearities and sensitivity to details.[9]

We focus in this work on the manganites, area where in recent years considerable progress has been made, both in theory and experiments.[6–8] In the late 1990's, it was predicted that many Mn oxides should be inhomogeneous at the nanoscale, due to the unveiling of tendencies toward electronic phase separation.[10–17] On the experimental front, the evidence for inhomogeneous states was rapidly gathered and it is by now widely accepted, with building blocks typically having small nanoscale sizes.[18–21] Subsequent theoretical work showed that similar tendencies can also occur after the inclusion of quenched disorder effects—caused, for instance, by chemical doping—near first-order phase transitions.[22,23] The key influence of quenched disorder was also observed in simulations of the one-orbital model for manganites including cooperative phonons[24,25] and also for two orbitals with Jahn-Teller phonons.[26,27] This key role of quenched disorder postulated by theory was observed experimentally using a Mn-oxide compound that can be prepared both in crystal ordered and disordered forms.[28–30] Remarkably, only the latter presents a colossal magnetoresistance (CMR) effect.

While the presence of quenched disorder was theoretically found to generate metal insulator transitions similar to those found experimentally, the actual existence of large magnetotransport effects is difficult to test in unbiased theoretical studies. Using toy models that have phase competition and first-order transitions, and supplementing the investigations with a random-resistor network approximation, huge magnetoresistances were obtained in resistance vs temperature profiles in excellent agreement with experiments.[31,32] However, it is certainly desirable to carry out similar investigations in more realistic models, of the double-exchange variety, and with quantum mechanical procedures to calcu-

 ©2006 The American Physical Society

late the conductances. Alas, this task is tremendously difficult with standard computational methods that rely on the exact diagonalization of the fermionic sector and the Monte Carlo simulation of the classical $t_{2g}$ spins.[6–8] The effort in this context grows as $N^4$, with $N$ the number of sites, severely limiting the clusters that can be studied. Since theory suggests that physics related with percolative phenomena is anticipated upon the introduction of magnetic fields in nanoclustered states,[6–8,25] large clusters must be used for accurate simulations. Fortunately, important progress has been made in recent years toward the development of a method to carry out these investigations.[33–36] The truncated polynomial expansion method (TPEM), has a CPU time that scales linearly with $N$ and, as a consequence, it is a promising technique for these investigations. Previous studies have shown that the $J_H=\infty$ one-orbital model with and without quenched disorder can be accurately studied.[33–37] However, the method has not been tested yet under some of the more severe circumstances needed for a realistic study, namely, the use of two active orbitals per site (*i.e.* the doubly degenerate $e_g$ sector of Mn ions) and/or with a finite Hund coupling.

It is important to remark that there are at least two other independent methods that have been proposed to improve on the exact diagonalization of the fermionic sector approach. (1) The hybrid Monte Carlo technique of Alonso *et al.*,[38] inspired in lattice gauge theory, that allows for calculations on lattices up to $16^3$ sites in the limit of $J_H=\infty$ and for one orbital,[39,40] and with a linear with $N$ increase in effort. (2) The method of Kumar and Majumdar[41] (and references therein) that has been already applied to a variety of models reaching $32\times32$ clusters for one orbital and at $J_H=\infty$. The scaling of this method is $N^3$. Our choice of the TPEM is motivated by the perception that a linear with $N$ cost is needed to handle the anticipated percolative physics that emerges when quenched disorder and phase competition occurs. Also it seems easier to implement than method (1) where auxiliary fields are needed. Nevertheless, this is not a critique on methods (1) and (2): they should be strongly pursued as well. Only future work can decide which method is the best for the type of problems described here.

There are many similarities between the TPEM and methods already used for band structure calculations. Even though the matrix diagonalization is $O(N^3)$, integrated quantities such as the total energy depend only upon the density or the density matrix, without the need to compute eigenstates. The density matrix becomes a sparse matrix that leads to a large decrease in complexity. As in the case of the TPEM, most band-structure $O(N)$ methods find a basis set that is localized and truncate the range of the interaction while ensuring accuracy and convergence.

For instance, the locally self-consistent multiple scattering (LSMS) method[42] is an all-electron real space approach to electronic structure calculations within the framework of the local density approximation (LDA) for large unit cells consisting of hundreds or thousands of atoms. Within this method the computational effort required to treat an $N$-atom large cell grows linearly with $N$, rather than with $N^3$ as in conventional LDA electronic structure methods. Density matrix methods have also been proposed.[43,44] Another class of methods use localized Wannier orbitals[45–48] which improve on the Car-Parrinello approach.[49] An efficient tight-binding method in molecular dynamics is discussed in Ref. 50. Reviews on this topic can be found in Refs. 51 and 52.

It is the main purpose of this paper to present a systematic study of the TPEM applied to models that are widely believed to be realistic for manganite investigations, in the clean limit. The conclusions indicate that the technique works properly for these investigations, contributing toward the ultimate goal of conducting a fully realistic simulation of the two-orbital double-exchange model including quenched disorder. The present results include a detailed analysis of both metallic and insulating phases on lattices as large as $48\times48$ sites, about 20 times larger in number of sites than it is possible to handle with exact diagonalization techniques. In addition, here it is discussed the existence of a huge magnetoresistance at low temperatures, in agreement with experiments for $(Nd_{1-y}Sm_y)_{1/2}Sr_{1/2}MnO_3$.[53] This phenomenon was theoretically studied before by Aliaga *et al.*[26] as well, although on much smaller systems. Nevertheless, the conclusions are similar: this somewhat exotic "low temperature" CMR phenomenon can be understood as a natural consequence of the existence of a first-order metal-insulator transition in the phase diagram and, thus, a clean-limit simulation is sufficient for this purpose. However, in our investigations it is also confirmed that these clean limit simulations are *not* able to generate the standard CMR effect above the Curie temperature using states that are homogeneous. Quenched disorder or strain fields are likely important for this purpose, which will be the subject of near future efforts.

The organization of the paper is simple. The theoretical aspects of the TPEM are briefly reviewed in Sec. II. The systematics of the TPEM in the case of the one-orbital model, with emphasis on the dependence with parameters and size effects is discussed in Sec. III. We also present physical results related with large magnetoresistance effects found at low temperatures, in large clusters. Then, in Sec. IV, the emphasis shifts to the two orbitals model, with an analogous study of TPEM performance and effects of magnetic fields. Conductances are evaluated for both models using the TPEM and reasonable results are observed. Overall, it is concluded that the TPEM is adequate for a frontal future attack of the CMR phenomenon using realistic models and quenched disorder.

## II. REVIEW OF THE TPEM

For completeness, here a brief review of the TPEM is presented following closely Ref. 37. Consider a model defined by a general Hamiltonian $\hat{H}=\Sigma_{ij\alpha\beta}c_{i\alpha}^{\dagger}H_{i\alpha,j\beta}(\phi)c_{j\beta}$, where the indices $i$ and $j$ denote a spatial index, while $\alpha$ and $\beta$ are internal degree(s) of freedom, e.g., spin and/or orbital. As in the case of spin-fermion models, the Hamiltonian matrix depends on the configuration of one or more classical fields, represented by $\phi$. Although no explicit indices will be used, the field(s) $\phi$ are supposed to have a spatial dependence. The partition function for this Hamiltonian is schematically given by $Z=\int d\phi\Sigma_n\langle n|\exp[-\beta\hat{H}(\phi)+\beta\mu\hat{N}]|n\rangle$,

where $|n\rangle$ are the eigenvectors of the one-electron sector, and the $\phi$ integral denotes the integration over all the classical fields. Here $\beta=1/(k_BT)$ is the inverse temperature. The number of particles (operator $\hat{N}$) is adjusted via the chemical potential $\mu$.

The procedure to calculate observables (energy, density, action, etc.) is the following. First, an arbitrary configuration of classical fields $\phi$ is selected as a starting point. The Boltzmann weight or action of that configuration $S(\phi)$ is calculated by diagonalizing the one-electron sector. Then, a small local change of the field configuration is proposed, so that the new configuration is denoted by $\phi'$ and its action is recalculated to obtain the difference in action $\Delta S=S(\phi')-S(\phi)$. Finally, this new configuration is accepted or rejected based on a Monte Carlo algorithm, such as Metropolis or heat bath, and the cycle starts again. In summary, in the standard algorithm (that we will denote here as DIAG) the observables are calculated using an exact diagonalization of the one-electron sector for every classical field configuration, and Monte Carlo integration for those classical fields.[6–8]

The TPEM replaces the diagonalization for a polynomial expansion as discussed below (details can be found in Refs. 33–35). It will be assumed that the Hamiltonian $H(\phi)$ is "normalized," which simply implies a rescaling in such a way that the normalized Hamiltonian has eigenvalues $\epsilon_v \in [-1,1]$. Simple observables can be divided in two categories: (i) those that do not depend directly on fermionic operators, e.g., the magnetization, susceptibility and classical spin-spin correlations in the double exchange model and (ii) those for which a function $F(x)$ exists such that they can be written as $A(\phi)=\int_{-1}^{1}F(x)D(\phi,x)dx$, where $D(\phi,\epsilon)=\Sigma_\nu\delta[\epsilon(\phi)-\epsilon_\nu]$, and $\epsilon_\nu$ are the eigenvalues of $H(\phi)$, i.e., $D(\phi,x)$ is the density of states of the system.

For category (i), the calculation is straightforward and simply involves the average over Monte Carlo configurations. Category (ii) includes the effective action or generalized Boltzmann weight and this quantity is particularly important because it is calculated at every MC step to integrate the classical fields. Therefore, we first briefly review how to deal with this type of observables. As Furukawa *et al.* showed, it is convenient to expand the function $F(x)$ in terms of Chebyshev polynomials [54,55] in the following way: $F(x)=\Sigma_{m=0}^{\infty}f_mT_m(x)$, where $T_m(x)$ is the $m$th Chebyshev polynomial evaluated at $x$. Let $\alpha_m=2-\delta_{m,0}$. The coefficients $f_m$ are calculated with the formula $f_m=\int_{-1}^{1}\alpha_mF(x)T_m(x)/(\pi\sqrt{1-x^2})$. The moments of the density of states are defined by

$$\mu_m(\phi)\equiv\sum_{\nu=1}^{N_{dim}}\langle\nu|T_m(H(\phi))|\nu\rangle, \tag{1}$$

where $N_{\mathrm{dim}}$ is the dimension of the one-electron sector. Then, the observable corresponding to the function $F(x)$ can be calculated using

$$A(\phi)=\sum_m f_m\mu_m(\phi). \tag{2}$$

In practice, the sum in Eq. (2) is performed up to a certain cutoff value $M$, without appreciable loss in accuracy as described in Refs. 33 and 34, and as extensively tested in the main sections of this paper for realistic manganite Hamiltonians. The calculation of $\mu_m$ is carried out recursively using $|\nu;m\rangle=T_m(H)|\nu\rangle=2H|\nu;m-1\rangle-|\nu;m-2\rangle$. These same vectors are used to calculate the moments. The process involves a sparse matrix-vector product, e.g., in $T_m(H)|\nu\rangle$, yielding a cost of $O(N^2)$ for each configuration, i.e., $O(N^3)$ for each Monte Carlo step. This represents an improvement in a factor $N$ compared with DIAG.

In addition, an extra improvement of the method described thus far has been proposed[35] based on two truncations: (i) of the sparse matrix-vector product and (ii) of the difference in action for local Monte Carlo updates. The resulting algorithm has an expected CPU time growing linearly with $N$. The first truncation is possible because of the form of the vectors $|\nu;m\rangle$. Indeed, for $m=0$ these are simply basis vectors that can be chosen with only one nonzero component. The $m=1$ vector is obtained by applying $T_1(H)=H$ to the basis vector. Since $H$ is sparse (consider, for instance, a nearest-neighbor hopping), the vector $|\nu;m=1\rangle$ will have nonzero elements only in the vicinity of $\nu$. For general $m$, the nonzero elements will propagate in what resembles a diffusion process. Note that we only have to keep track of the nonzero indices to perform the sparse matrix-vector product. Since we are only discarding null terms, this truncation does not introduce any approximation. It is possible to go a step further and discard not only zero elements but elements smaller than a certain threshold denoted by $\epsilon_{\mathrm{pr}}$. In this case, the results are approximate, but the exact results are recovered in the limit $\epsilon_{\mathrm{pr}}\to 0$. In this paper, the dependence of results with various values for this cutoff (and the one described below) is discussed.

The second truncation involves the difference in effective action, which is calculated very frequently in the Monte Carlo integration procedure. The function corresponding to the effective action for a configuration $\phi$ is defined by $F^S(x)=-\ln\{1+\exp[-\beta(x-\mu)]\}$ and $S(\phi)$ admits an expansion as in Eq. (2), with coefficients $f_m^S$ corresponding to $F^S(x)$. In practice, only the difference in action, $\Delta S=S(\phi')-S(\phi)$ has to be computed for every change of classical fields. Since this operation requires calculating two sets of moments, for $\phi$ and $\phi'$, the authors of Ref. 35 have also developed a truncation procedure for this trace operation controlled by a small parameter $\epsilon_{\mathrm{tr}}$. This truncation is based on the observation that if $\phi$ and $\phi'$ differ only in very few sites (as is the case with local Monte Carlo updates), then the corresponding moments will differ only for certain indices allowing for a significant reduction of the computational effort. Again, the exact results are recovered for $\epsilon_{\mathrm{tr}}\to 0$, so this approximation is controllable.

Another key advantage of the TPEM is that it can be parallelized, because the calculation of the moments in Eq. (1) for each basis ket $|\nu\rangle$ is independent. Thus, the basis can be partitioned in such a way that each processor calculates the moments corresponding to a portion of the basis. It is important to remark that the data to be moved between different nodes are small compared to calculations in each node: communication among nodes is mainly done here to add up all the moments. The possibility of parallelizing this

algorithm can be contrasted with the conventional method where a matrix diagonalization is performed at every Monte Carlo step; in that case the calculations must be serial because it is difficult to make an efficient parallelization of the matrix diagonalization.

## III. RESULTS FOR THE ONE BAND MODEL

### A. Definition

After introducing the computational method, we will now focus on its performance starting with the one-orbital model for manganites. Historically, this model was among the first proposed for Mn oxides and it is still widely used, although it does not incorporate the two orbitals $e_g$ of relevance in Mn ions. This more involved two-orbital version will be studied in the next section.

The one orbital Hamiltonian used in this study is given by

$$H_{1b} = -t \sum_{\langle ij\rangle,\alpha} (c^{\dagger}_{i,\alpha} c_{j,\alpha} + \text{H.c.}) - J_H \sum_{i,\alpha,\beta} c^{\dagger}_{i,\alpha} \sigma_{\alpha,\beta} c_{i,\beta} + J_{\text{AF}} \sum_{\langle ij\rangle} \mathbf{S}_i \cdot \mathbf{S}_j, \quad (3)$$

where $c^{\dagger}_{i,\alpha}$ creates an electron at site $i$ with spin $\alpha$, $\sigma$ are the Pauli spin matrices, $\mathbf{S}_i$ is the total spin of the $t_{2g}$ electrons (assumed to be localized and classical), $\langle ij\rangle$ indicates summing over nearest neighbor sites, $t$ is the nearest neighbor hopping amplitude for the movement of electrons ($t$ also sets the energy unit), $J_H > 0$ is the Hund coupling, and $J_{\text{AF}} > 0$ is the antiferromagnetic coupling between the localized spins. The study carried out in this manuscript is based on the *clean* limit, namely, the couplings that appear in the Hamiltonian do not have a site index, which would be necessary if quenched disorder is incorporated. The study of realistic models including disorder will be carried out in a future investigation, since it represents an order of magnitude extra effort due to the average over disorder configurations.

Here and in the rest of the paper, spatial indices will always be denoted without arrows or bold letters independently of the dimension. Also the notation $i+j$ is meant to represent the lattice site given by the vectorial sum of the vectors corresponding to $i$ and $j$, respectively.

### B. TPEM performance

#### *1. Test of the TPEM in small systems*

As explained before, the TPEM has three controlling parameters $M$, $\epsilon_{\text{pr}}$, and $\epsilon_{\text{tr}}$. In the limit when the first parameter runs to infinity, and the other two to zero, the exact results are recovered. For the TPEM to be useful, accurate results must be obtained for values for these parameters that allow for a realistic computational study. In Fig. 1(a), the dependence of the zero-momentum spin structure factor, of relevance for ferromagnetism, is shown vs temperature, using a $12^2$ cluster and the values of $J_H$ and $J_{\text{AF}}$ indicated. In this case, it is expected that a FM state will form at low temperatures, as observed numerically. Results for many values of $M$ are shown, at fixed values of $\epsilon_{\text{pr}}$ and $\epsilon_{\text{tr}}$. Clearly, $M=10$ only captures the low and high temperature limits, but it is not

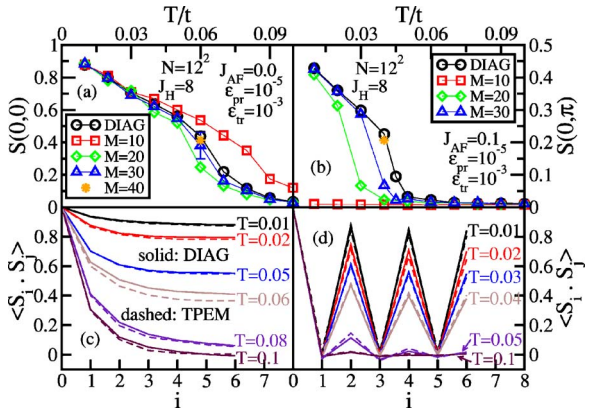


FIG. 1. (Color online) Dependence of the TPEM algorithm results on the number of terms $M$ in the expansion. Shown are the spin structure factors at the momenta characteristic of (a) the FM state and (b) the flux state, normalized to 1 and 0.5, respectively, for the perfect states. Results are obtained on a $12\times12$ lattice and they are compared with the numbers gathered using the exact diagonalization algorithm, all calculated at density $\langle n\rangle=0.5$. (a), (c) correspond to $J_{\text{AF}}=0.0$ and (b), (d) to $J_{\text{AF}}=0.1$. Measurements were taken every 10 steps of a MC run of 2000 total iterations, after discarding 2000 steps for thermalization. A random starting configuration is used for each $T$. In (a), at the most difficult temperature, $T=0.06$, where critical fluctuations are strong, the result shown was confirmed using several different starting configurations, including ordered ones. The average $S(0,0)$ obtained by this procedure was very similar among the several starts. The shown error bars at this temperature and $M=30$ mainly arise from the expected critical fluctuations. More details are provided in Sec. III B 3. In (b), a good convergence at $T=0.04$ is only achieved by using 40 moments with $\varepsilon_{\text{pr}}=10^{-7}$ and $\varepsilon_{\text{tr}}=10^{-5}$ and the result is shown with an orange star just below the exact result. In (c), the TPEM parameters used are $M=30$, $\varepsilon_{\text{pr}}=10^{-5}$, and $\varepsilon_{\text{tr}}=10^{-3}$, except at $T=0.06$, where the convergence is achieved by using 40 moments with $\varepsilon_{\text{pr}}=10^{-7}$ and $\varepsilon_{\text{tr}}=10^{-5}$. In (d), all the results shown were obtained with $M=30$, $\varepsilon_{\text{pr}}=10^{-5}$, and $\varepsilon_{\text{tr}}=10^{-3}$, and solid lines represent the DIAG results while the dashed lines are the TPEM results.

accurate near the critical temperature. The results for $M=20$ are much better, but still there is a visible discrepancy near the region where $S(0,0)$ changes the fastest. However, for $M=30$ and 40, fairly accurate results are obtained. In Fig. 1(c), it is shown that even the spin correlations at the largest distances are accurately reproduced with $M=40$ terms in the expansion. The issue of error bars shown in the figure will be discussed in Sec. III B 3.

In Fig. 1(b), similar results are presented but now for the spin-structure-factor corresponding to the "flux" phase—nearest-neighbor spins at 90° forming a staggered arrangement of nonzero plaquette fluxes. This phase appears at $n=0.5$ with increasing $J_{\text{AF}}$, as reported in previous investigations. [10,56,57] In this case, $M=10$ and even 20 produces results dramatically different from those of DIAG. However, for $M=30$ discrepancies are observed only in a range of temperatures near the critical transition, with low and high temperatures under control. Finally, $M=40$ leads to very accurate results, as in case (a). Even the spin correlations are under well control for this number of terms in the expansion

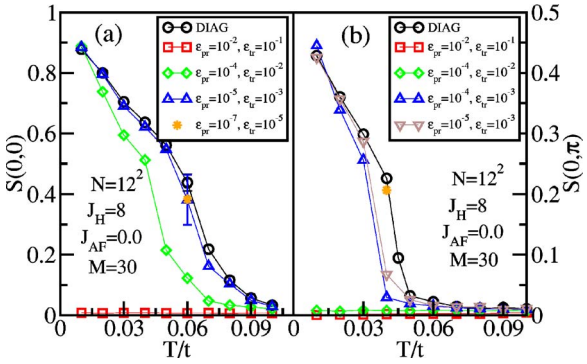


FIG. 2. (Color online) $\varepsilon$ dependence of the TPEM algorithm results ($M=30$) for a $12\times12$ lattice, compared with the exact (DIAG) results. Both are obtained at density $\langle n\rangle=0.5$, using (a) $J_{AF}=0.0$ and (b) $J_{AF}=0.1$. Measurements were taken at every 10 steps of a 2000 MC steps total run, after 2000 steps for thermalization. In (b), the convergence at $T=0.04$ is achieved by using 40 moments with $\varepsilon_{pr}=10^{-7}$ and $\varepsilon_{tr}=10^{-5}$, as shown with an orange star just below the exact result. The starting configurations and error bar convention is as in Fig. 1.

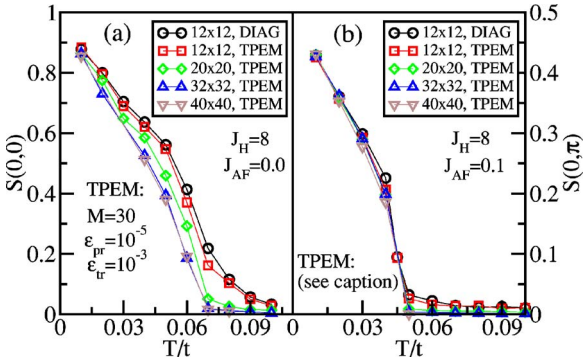


FIG. 3. (Color online) Lattice size dependence of the TPEM algorithm results for the lattices and parameters shown, working at density $\langle n\rangle=0.5$ and using (a) $J_{AF}=0.0$ and (b) $J_{AF}=0.1$. Measurements were taken at every 10 steps of a 2000 MC total steps run, after discarding 2000 MC steps for thermalization. For the $20\times20$ lattice and larger, the starting configuration used was a perfect FM state. In (b), the starting configuration used is a random one except at $T=0.04$ where the starting configuration is chosen to be a perfect flux state for faster convergence. In addition, for lattices except $40\times40$, the convergence at $T=0.04$ is achieved by using 40 moments with $\varepsilon_{pr}=10^{-7}$ and $\varepsilon_{tr}=10^{-5}$, while for other temperatures $M=30$ with $\varepsilon_{pr}=10^{-5}$ and $\varepsilon_{tr}=10^{-3}$ were sufficient. For the lattice $40\times40$, $M=40$ with $\varepsilon_{pr}=10^{-6}$ and $\varepsilon_{tr}=10^{-4}$ were used for all temperatures.

[see Fig. 1(d)]. The range $M\sim30-40$ appears systematically in our investigations, and it is expected to provide safe values of $M$ for studies of the type of spin-fermion models under investigation in manganites.

In Fig. 2, a study of the dependence of results with $\epsilon_{pr}$ and $\epsilon_{tr}$ is presented, working at $M=30$. From Fig. 2, clearly there are large $\epsilon$'s that lead to unphysical results, but with decreasing values an accurate evaluation of observables is reached. In this and other investigations, values such as $\epsilon_{pr}=10^{-5}$ and $\epsilon_{tr}=10^{-3}$ are generally found to be accurate, with only a few exceptions.

### 2. Dependence of results on lattice sizes

An approximate method that depends on some parameters, such as in the case of the TPEM, is practical only if by fixing those parameters on small systems, their values still provide accurate numbers as the lattice sizes increase. A qualitative way to carry out this test is to perform the studies on large clusters and see that all the trends and approximate numbers remain close to those known to be accurately obtained on small systems, or expected from other techniques or physical argumentations. Figures 3(a) and 3(b) supports the notion that TPEM indeed behaves properly in this respect, namely the range of $M$ and $\epsilon$'s identified in the previous subsection are sufficient to produce qualitatively similar results even when the number of sites grows by a factor 10. In (a), the expected size dependence corresponding to a second order FM transition is found. For a $40\times40$ cluster, the Curie temperature appears located at $T\sim0.07$. In (b), the size dependence is almost negligible. The transition is far sharper for the paramagnetic-flux transition, as already noticed in Fig. 2(b). This is an intriguing feature that will be investigated in future work: while the first-order low-temperature metal-insulator transitions are clear and well established in realistic models for manganites, the presence of first-order transitions between ordered and disordered phases varying temperature is far less obvious, and TPEM studies on large lattices can properly address this issue. For our current purposes, here it is sufficient to state that the TPEM appears to behave properly with increasing lattice sizes, both in metallic and insulating regimes.

At this point a clarification is important. In principle, two-dimensional systems should not show true critical temperatures due to the Mermin-Wagner theorem. However, it is well known that in systems where the Mermin-Wagner theorem applies, such as the two-dimensional NN Heisenberg model, the antiferromagnetic spin correlation length exponentially diverges with decreasing temperature. An exponential behavior, defines via the exponent a temperature scale $T^*$ below which the correlations are much larger than any lattice size that can be practically studied numerically. This may seem to be a problem, but it is not: very large correlation lengths also render the system very susceptible to small perturbations. In particular, we have shown that tiny deviations from the fully symmetric Heisenberg model, such as introducing Ising anisotropies, stabilize $T^*$ into a true critical temperature. In fact, simulations performed with Ising anisotropies typically reveal no important differences with the results obtained with fully vector models on finite systems. Small couplings in the third direction play a similar role. As a consequence, for all practical purposes the critical behavior observed in the present studies describes properly the expected physics of manganite models, which are always embedded in three dimensional environments, and that have small anisotropies. A final note on this subject: The CE phase of manganites, notation introduced long ago by Wollan and Koeller,[58] can show a finite-temperature transition even in two dimensions, since the order parameter for charge order can be Ising type (see Fig. 4).

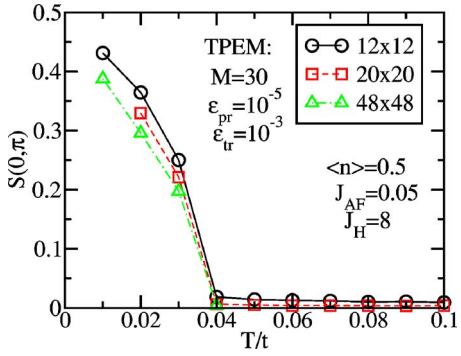


FIG. 4. (Color online) Spin structure factor vs $T$ for $J_{AF}=0.05$ using the lattice sizes and parameters shown in the figure.

The CPU time needed to obtain the results shown in this subsection follows the expected trends reported in previous investigations (see Table I). In particular, the TPEM time needed for a $32\times32$ cluster is comparable to the DIAG time on a $12\times12$ cluster, a very encouraging result. Of course, this comparison will be even more favorable to the TPEM with increasing number of CPU's for parallelization.

### *3. Analysis of error bars*

In this subsection, a detailed analysis of the error bars that arise in the TPEM simulation will be carried out. We focus here on only one set of parameters, and temperatures below and right at criticality. However, investigations for other set of couplings have revealed that the conclusions are similar, and the order of magnitude of the error bars comparable. As a consequence, rather than complicating all the figures in the manuscript, we simply here discuss in detail a couple of cases and, then, throughout the paper similar error bars must be assumed in the ordered and critical regions unless otherwise stated.

The error bars are calculated using the data blocking technique,[59] where data is averaged over each of the $L=N/K$ blocks, where $N$ is the total number of measurements and $K$ is the block size. The size $K$ of the blocks have been varied from 1 to 1000 and the asymptotic value of the standard deviation is calculated [e.g., inset of Fig. 5(a)] for each $K$, setting an upper limit for the error bars. The calculated autocorrelation times have also been observed to coincide with the value of the block size $K$ for which the standard deviation $\sigma$ starts to flatten.

TABLE I. Comparison of the CPU times for the algorithms indicated, using an Intel Pentium 4 (clock speed 3.06 Gz) computer. Shown are results for different square lattices of size $L\times L$, assuming 2000 MC steps for thermalization, and 2000 MC steps for measurements (taken every 10 MC steps). Since the TPEM can be parallelized, some results were obtained using more than one CPU, as indicated.

| $L$ | Algorithm | No. of CPUs | CPU time (h) |
|---|---|---|---|
| 12 | DIAG | 1 | 19.48 |
| 12 | TPEM | 2 | 5.46 |
| 20 | TPEM | 2 | 18.08 |
| 32 | TPEM | 8 | 25.92 |

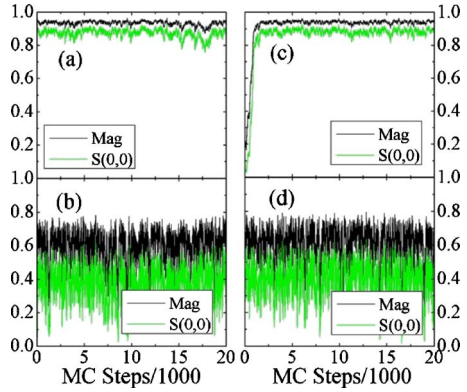


FIG. 5. (Color online) Analysis of MC error bars (standard deviation) with TPEM for parameters $M=30$, $\epsilon_{pr}=10^{-5}$, and $\epsilon_{tr}=10^{-3}$. (a) and (b) results using a FM starting configuration; (c) and (d) using a PM starting configuration. (a) $T=0.01$, $\langle\text{mag}\rangle=0.934$ with $\sigma_{\text{mag}}=0.003$ and $\langle S(0,0)\rangle=0.872$ with $\sigma_{S(0,0)}=0.005$. (b) $T=0.06$, $\langle\text{mag}\rangle=0.603$ with $\sigma_{\text{mag}}=0.007$ and $\langle S(0,0)\rangle=0.371$ with $\sigma_{S(0,0)}=0.008$. (c) $T=0.01$, $\langle\text{mag}\rangle=0.940$ with $\sigma_{\text{mag}}=0.001$ and $\langle S(0,0)\rangle=0.883$ with $\sigma_{S(0,0)}=0.002$. (d) $T=0.06$, $\langle\text{mag}\rangle=0.616$ with $\sigma_{\text{mag}}=0.006$ and $\langle S(0,0)\rangle=0.388$ with $\sigma_{S(0,0)}=0.007$. The approximate number of independent Monte Carlo steps, obtained with the data-blocking technique (Ref. 59), is 100 for case (d).

In Fig. 5, the MC time evolutions of the magnetization and $S(0,0)$ for the parameters corresponding to Fig. 1(a) are presented. Shown are results using both ordered and disordered starting configurations. In the case of the ordered start and low temperature $T=0.01$, the fluctuations are clearly very small in both quantities. If the starting configuration is random, there is a rapid thermalization and the results converge to the ordered state as, of course, it must occur. The error bars are very small. This is characteristic of all the studies reported in this paper in the low temperature regime below critical temperatures.

As expected, much stronger fluctuations occur in the case of $T=0.06$, which corresponds to the critical regime in Fig. 1(a). While results are independent of the starting configuration, the fluctuations are large. For a magnetization (or other order parameters) normalized to one, the errors are typically about 0.1 for the $12\times12$ cluster here studied. Another simple procedure to judge the magnitude of error bars is to analyze the results obtained at similar temperatures, starting with different random configurations. This is the case of Fig. 1, for instance. The fluctuations from temperature to temperature are related to the error bars of the simulation.

## C. Phase diagram

Using the TPEM, the phase diagram of the one-orbital model for manganites at $\langle n\rangle=0.5$ was obtained (see Fig. 6). The transition between the FM and Flux states at low temperatures is of first order. In fact, in the absence of quenched disorder the zero temperature result can be obtained by using the perfect classical spin configurations for both the FM and flux states, and calculating their energy vs $J_{AF}$ (not shown).

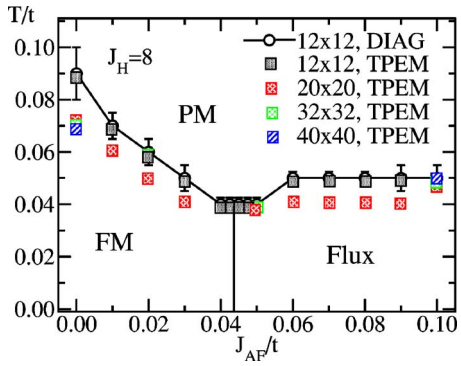


FIG. 6. (Color online) Phase diagram at $\langle n\rangle=0.5$, varying temperature and $J_{AF}$. Results are shown for a $12\times12$ lattice using both DIAG and TPEM techniques, and for larger lattices using TPEM, as indicated. The tilting of the first-order low-temperature FM-flux line emerges from a combination of finite-$T$ MC simulation results and the $T=0$ energy comparison between FM and flux phases. Its intuitive origin remains to be clarified in future work.

By this procedure the zero-temperature critical $J_{AF}$ was found to be close to 0.03. Raising the temperature, this transition line is not vertical, but has a tilting. Figure 6 shows that the estimated critical temperatures do not present severe size effects, and the TPEM can be comfortably used at least up to $40\times40$ clusters. The presence of a first-order transition in the competition between the FM and flux phases is in qualitative agreement with several previous investigations that have shown similar trends both for the one- and two-orbital models, at any electronic density.[6–8] This transition is expected to be severely affected by the influence of quenched disorder, and this issue will be investigated in the near future. The critical temperatures in Fig. 6 were estimated from the behavior of the spin structure factors at the two momenta of relevance for the FM and Flux phases, as shown in Fig. 7.

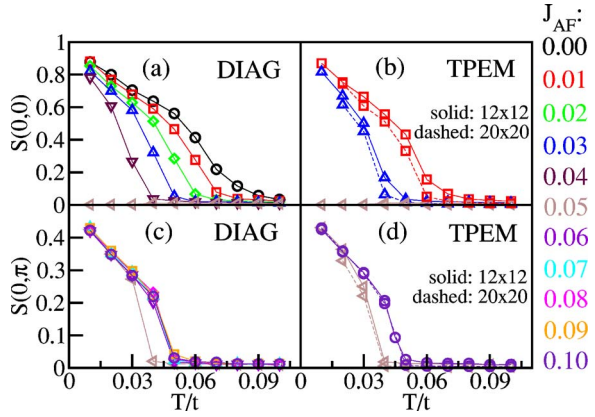


FIG. 7. (Color online) Examples of the criteria used in the calculation of the critical temperatures in Fig. 6. (a) and (c): Spin structure factors at the momenta of relevance vs temperatures, for many values of $J_{AF}$, as indicated, using the DIAG technique on a $12\times12$ cluster. (b) and (d): Same as in (a) and (c) except the technique used here is the TPEM. Shown are some of the results for $12\times12$ and $20\times20$, as indicated in the figure.

### D. Density of states

In this section, it is shown that the density-of-states (DOS) can be reproduced properly by the TPEM. This is nontrivial, since it may be suspected that a method based on an expansion of the DOS may have problems in an insulating phase due to the rapid changes in the DOS near the gap.[60] To our knowledge, this is the first time that the TPEM has been applied to an insulator. The discussion in this subsection shows that the technique works satisfactorily.

In general, the density-of-states for a configuration of classical fields $\phi$ is given by

$$N_\phi(\omega)=\sum_\lambda \delta(\omega'-\epsilon_\lambda), \tag{4}$$

with $\omega'=(\omega-b)/a$, and where $a$ and $b$ are the parameters that normalize the Hamiltonian in such a way that the new eigenvalues are in the interval $[-1,1]$. These constants are given by $a=(E_{max}-E_{min})/2$ and $b=(E_{max}+E_{min})/2$, where $E_{max}$ and $E_{min}$ are the maximum and minimum eigenvalues of the Hamiltonian. Then, following the discussion of Sec. II, the corresponding function $F(x)$ for the density-of-states in the expression

$$A(\phi)=\int_{-1}^{1} F(x)D(\phi,x)dx \tag{5}$$

is the $\delta$ function

$$F(x)=\delta(\omega'-x). \tag{6}$$

In the expansion $F(x)=\Sigma_{m=0}^{\infty} f_m T_m(x)$, by using the expression for the coefficients $f_m=\int_{-1}^{1}\alpha_m F(x)T(x)/(\pi\sqrt{1-x^2})$, the final result for the density-of-states becomes[61]

$$N_\phi(\omega)=\frac{\sum_m \alpha_m T_m(\omega')\mu_m(\phi)}{\pi\sqrt{1-\omega'^2}}. \tag{7}$$

This sum is truncated to a certain cutoff $M$ and such an abrupt truncation results in unwanted Gibbs oscillations, as shown, e.g., in Fig. 8 for $M=30$. This problem may be avoided by multiplying the moments by damping factors if needed.[62]

The results for the density-of-states of the flux phase are shown in Fig. 8. Clearly, even at $M=30$ there is a very good agreement between the DOS calculated exactly and with TPEM (with the exception of the in-gap Gibbs oscillations). Increasing $M$ further, even this effect disappears. Using a $40\times40$ lattice, the results are almost the same as those observed on the smaller system. It is concluded that the TPEM can produce the DOS of insulating states accurately, and the method can be used to study phase competition between metals and insulators.

### E. Conductances: Comparison TPEM vs DIAG, and results with increasing lattice sizes

To compare theory with experiments, it is crucial to evaluate the conductance of the cluster under study. Its temperature and magnetic field dependence will clarify whether

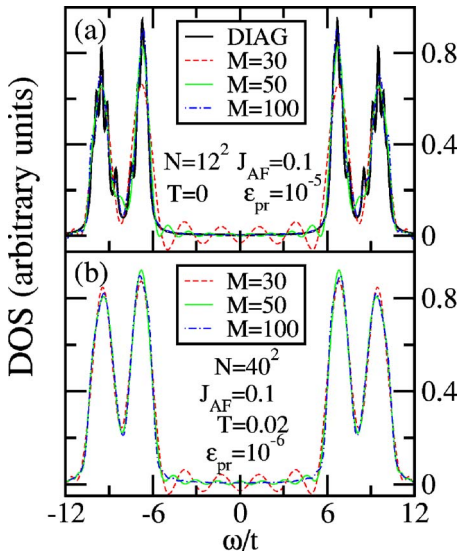


FIG. 8. (Color online) (a) Density-of-states calculated for a perfect Flux state using both the DIAG and TPEM methods for a lattice of size $12\times12$. In order to get the DOS accurately, even removing the Gibbs oscillations, one needs larger number of moments than what is usually required for other observables. (b) Monte Carlo results for the density-of-states obtained from simulations performed on a $40\times40$ lattice. In this case the last configuration of the MC run has been used to calculate the density-of-states at $T=0.02$.

the double-exchange models for manganites contain the essence of the CMR phenomenon. The conductance calculation here follows the steps previously extensively discussed by Vergés *et al.*, and it basically relies on the Landauer formalism that links conductance with transmission. We refer the readers to original references for more details (see, for instance, Ref. 63, and reference therein). In Fig. 9, the conductance and its inverse (resistance) are shown as a function of temperature for the model on a $12\times12$ cluster that can be solved both with DIAG and TPEM. The agreement between the results obtained with both techniques is excellent, at the

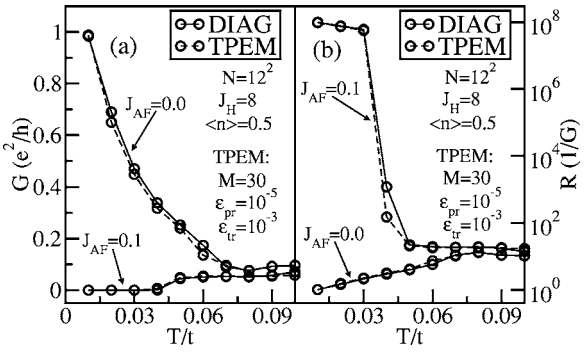


FIG. 9. (a) Conductance and (b) resistance (1/conductance) vs temperature for a $12\times12$ lattice, calculated with both DIAG and TPEM algorithms showing that the results agree. The couplings used are $J_{AF}=0.0$ and $J_{AF}=0.1$ as indicated, and the density is $\langle n\rangle=0.5$. The convergence at $T=0.04$ is achieved by using 40 moments with $\varepsilon_{pr}=10^{-7}$ and $\varepsilon_{tr}=10^{-5}$, as discussed in previous figures captions.

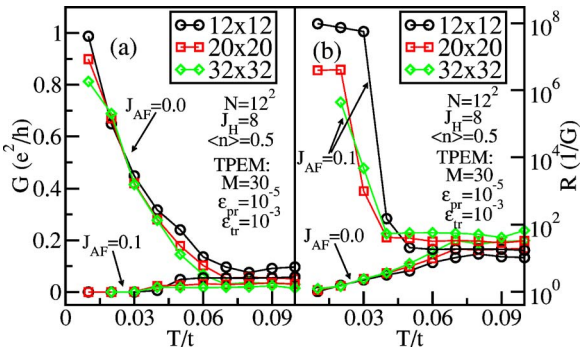


FIG. 10. (Color online) (a) Conductance and (b) resistance (1/conductance) vs temperature calculated with the TPEM algorithm at $J_{AF}=0.0$ and $J_{AF}=0.1$, $\langle n\rangle=0.5$, and for the cluster sizes shown in the figure. The figure shows that the conductance does *not* suffer from strong size effects. The convergence at $T=0.04$ for the $12\times12$ lattice was achieved by using 40 moments with $\varepsilon_{pr}=10^{-7}$ and $\varepsilon_{tr}=10^{-5}$, as discussed elsewhere.

two values of $J_{AF}$ shown (one in the FM and the other in the flux phase). Thus, the conductance calculation does not present an obstacle in the use of the TPEM.

With increasing lattice size, the TPEM conductance behaves smoothly and the finite-size effects are small (see Fig. 10), with the only exception of the insulating flux phase regime at low temperatures where the $12\times12$ cluster results appear appreciably different from those on larger systems. Considering the small value of the conductance in this insulating regime and the subsequent convergence of the flux-phase resistance between the $20\times20$ and $32\times32$ clusters, this appears to be only a minor issue.

### F. Influence of magnetic fields in the clean limit and partial conclusions

As discussed in the Introduction, it is important to investigate if the models studied here, in the clean limit, present a large magnetoresistance effect. Previous studies by Aliaga *et al.*[26] on $4\times4$ clusters, suggested that the "low temperature" large magnetoresistance experimentally observed in some manganites[53] can be explained by double-exchange models in the clean limit. This result is important and deserves to be confirmed using larger clusters. Here, the case of the one-orbital model is analyzed, with results shown in Fig. 11 (two orbitals will be studied later in this paper). The value of $J_{AF}$ was chosen to be on the insulating side (flux phase) of the phase diagram Fig. 6, but close to the first-order transition separating the metal from the insulator. The application of "small" magnetic fields favors the FM state over the flux state and that manifests as a sharp transition from the metal to the insulator, for values of the magnetic field that appear abnormally small in the natural units of the problem. Thus, this model presents a huge negative magnetoresistance, an encouraging result that shows theory is in the right track to understand manganites. The effect shown in Fig. 11 is caused by the proximity in energy of two states with quite different properties, i.e., there is a hidden small energy scale in the problem.

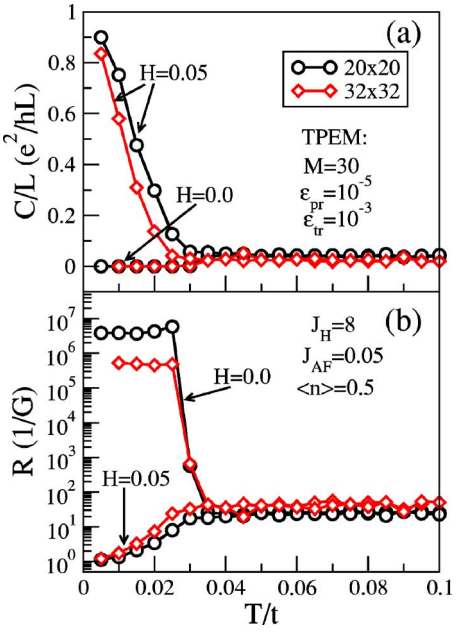


FIG. 11. (Color online) (a) Conductance vs temperature for lattices of sizes $20\times20$ and $32\times32$, with and without magnetic fields. (b) Resistance vs temperature calculated by taking the inverse of the conductance in (a). Close to the first-order transition in the phase diagram, a small magnetic field can destabilize the insulating flux state into a metallic FM state. For each temperature, 1000 thermalization and 2000 measurements MC steps were used, with actual measurements taken at every 10 steps.

However, note that the standard large finite-temperature magnetoresistance traditionally studied in Mn oxides cannot be understood with clean limit models, as shown in Fig. 11: the zero magnetic-field resistivity does not have the large peak near Curie temperatures characteristic of CMR manganites. Future work using the TPEM will analyze whether this more traditional CMR effect can be obtained including quenched disorder.

Overall, it can be safely concluded that the study of the one-orbital model with the TPEM has proven that the technique works properly, and that the FM vs flux competition occurs via a first-order metal-insulator transition. This regime is ideal for the analysis of the influence of quenched disorder in future calculations.

## IV. RESULTS FOR THE TWO-BAND MODEL

### A. Definition

In this effort, the two-orbital model for manganites was also investigated using the TPEM. The two orbitals arise from the $e_g$ orbitals that are active at the Mn ions in Mn oxides, as extensively discussed before.[6–8] The overall conclusion of this section is that the TPEM is also a good approximation to carry out computational studies, conclusion similar to that reached for only one active orbital. The Hamiltonian for this model is[6–8]

$$H_{2b} = \sum_{\gamma,\gamma',i,\alpha} t^{\alpha}_{\gamma\gamma'} \mathcal{S}(\theta_i,\phi_i,\theta_{i+\alpha},\phi_{i+\alpha}) c^{\dagger}_{i,\gamma} c_{i+\alpha,\gamma'} + \lambda \sum_i (Q_{1i}\rho_i + Q_{2i}\tau_{xi} + Q_{3i}\tau_{zi}) + \sum_i \sum_{\alpha=1}^{\alpha=3} D_\alpha Q^2_{\alpha i}, \quad (8)$$

where the factor that renormalizes the hopping in the $J_H=\infty$ limit is

$$\mathcal{S}(\theta_i,\phi_i,\theta_j,\phi_j) = \cos\left(\frac{\theta_i}{2}\right)\cos\left(\frac{\theta_j}{2}\right) + \sin\left(\frac{\theta_i}{2}\right)\sin\left(\frac{\theta_j}{2}\right) e^{-i(\theta_i-\theta_j)}. \quad (9)$$

The parameters $t^{\alpha}_{\gamma\gamma'}$ are the hopping amplitudes between the orbitals $\gamma$ and $\gamma'$ in the direction $\alpha$. In this paper, we restrict ourselves to two dimensions, such that $t^x_{aa}=-\sqrt{3}t^x_{ab}=-\sqrt{3}t^x_{ba}=3t^x_{bb}=1$, and $t^y_{aa}=\sqrt{3}t^y_{ab}=\sqrt{3}t^y_{ba}=3t^y_{bb}=1$. $Q_{1i}$, $Q_{2i}$, and $Q_{3i}$ are normal modes of vibration that can be expressed in terms of the oxygen coordinate $u_{i,\alpha}$ as

$$Q_{1i} = \frac{1}{\sqrt{3}}[(u_{i,z}-u_{i-z,z}) + (u_{i,x}-u_{i-x,x}) + (u_{i,y}-u_{i-y,y})],$$

$$Q_{2i} = \frac{1}{\sqrt{2}}(u_{i,x}-u_{i-x,x}),$$

$$Q_{3i} = \frac{2}{\sqrt{6}}(u_{i,z}-u_{i-z,z}) - \frac{1}{\sqrt{6}}(u_{i,x}-u_{i-x,x}) - \frac{1}{\sqrt{6}}(u_{i,y}-u_{i-y,y}).$$

Also, $\tau_{xi}=c^{\dagger}_{ia}c_{ib}+c^{\dagger}_{ib}c_{ia}$, $\tau_{zi}=c^{\dagger}_{ia}c_{ia}-c^{\dagger}_{ib}c_{ib}$, and $\rho_i=c^{\dagger}_{ia}c_{ia}+c^{\dagger}_{ib}c_{ib}$. The constant $\lambda$ is the electron-phonon coupling related to the Jahn-Teller distortion of the $MnO_6$ octahedron.[1,3–8,15] Regarding the phononic stiffness, and in units of $t^x_{aa}=1$, the $D_\alpha$ parameters are $D_1=1$ and $D_2=D_3=0.5$, as discussed in previous literature.[26] The rest of the notation is standard. In our effort here, the emphasis is on the case $\lambda=0$ believed to be of sufficient relevance to deserve a special study since it already contains[26] a competition between FM metallic and CE insulating states at $\langle n\rangle=0.5$. Thus, this is an excellent testing ground for the TPEM, particularly having in mind the next challenge involving a TPEM study in the presence of quenched disorder. However, briefly some results at nonzero $\lambda$ will also be shown.

### B. TPEM performance

#### *1. Test of the TPEM in small systems*

As in the case of the one-orbital model, the analysis starts here by comparing DIAG and TPEM results on small systems. Figure 12 contains the magnetization (in absolute value, and coming from the classical spins) vs temperature. The results in (a) and (c) were obtained at $J_{AF}=0.0$, $\lambda=0$, and $\langle n\rangle=0.5$, a regime known to develop ferromagnetism at low temperatures.[26] Indeed, both methods show a nonzero value for the magnetization. The dependence with the TPEM

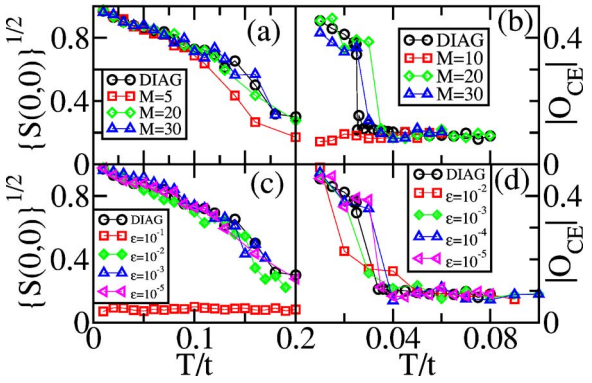


FIG. 12. (Color online) Convergence of the structure factors, varying the parameters of the TPEM algorithm. (a) Magnetization $|M|=\sqrt{S(0,0)}$ vs $T/t$ at $J_{AF}=0.0$ using the DIAG method and TPEM with $\epsilon_{pr}=10^{-5}$, $\epsilon_{tr}=10^{-6}$, and the values of $M$ indicated. (b) Order parameter associated with the CE phase $|O_{CE}|=\sqrt{S(\pi,0)}$ vs $T/t$ at $J_{AF}=0.2$ using the DIAG method and TPEM with $\epsilon_{pr}=10^{-5}$, $\epsilon_{tr}=10^{-6}$, and the values of $M$ indicated. (c) Magnetization $|M|=\sqrt{S(0,0)}$ vs $T/t$ at $J_{AF}=0.0$ using the DIAG method and TPEM with $M=20$ and $\epsilon_{tr}=10^{-6}$, varying $\epsilon_{pr}=\epsilon$ as indicated. (d) Order parameter of the CE phase $|O_{CE}|=\sqrt{S(\pi,0)}$ vs $T/t$ at $J_{AF}=0.2$ using the DIAG method and TPEM with $M=20$, $\epsilon_{tr}=10^{-6}$, varying $\epsilon_{pr}=\epsilon$ as indicated. All calculations were done on a $12\times12$ lattice, using 1000 Monte Carlo steps for thermalization and 1000 for measurements.

parameters indicates that a $M$ of approximately 30 or higher is sufficient to get accurate results. This is a conclusion that also appears in (b) where the case of a CE state is studied, which is stabilized with increasing $J_{AF}$. Regarding the other TPEM parameters, (d) shows that $\epsilon_{pr}=10^{-5}$, as used for the one-orbital case, leads to accurate results. Overall, it seems that the same set of parameters deduced from the one-orbital model investigations can also be used for two orbitals, an interesting simplifying result.

#### *2. Dependence of results on lattice sizes*

Figure 13 illustrates the dependence of results on lattice sizes. The systematic behavior is similar to that observed in the case of the one-orbital model at the same density $\langle n\rangle=0.5$. In (a) results for the magnetization vs temperature indicate the existence of a FM state at low temperatures, as well as small finite-size effects when the $20\times20$ and $32\times32$ clusters are compared. Even less pronounced size effects are found in the CE regime, increasing $J_{AF}$ as shown in (b). There is no indication that the TPEM deteriorates with increasing lattice size, providing hope that this method will be strong enough to handle the introduction of quenched disorder in future studies.

### C. Phase diagram

#### *1. Results without phonons*

To further test the TPEM, the phase diagram of the two-orbital model at $\lambda=0$ and $\langle n\rangle=0.5$ was obtained. Also at very low temperature, the energy was found as a function of $J_{AF}$.

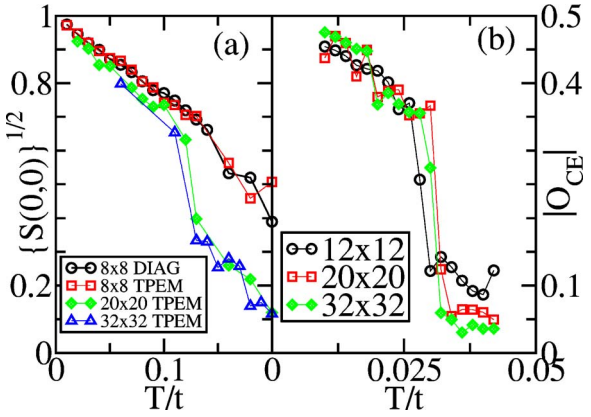


FIG. 13. (Color online) Lattice size dependence of the square root of the structure factors at the momenta characteristic of (a) a FM state, $\mathbf{k}=(0,0)$ and $J_{AF}=0.0$, and (b) a CE phase, $\mathbf{k}=(\pi,0)$ and $J_{AF}=0.2$. Results were obtained with the TPEM with $M=20$, $\epsilon_{pr}=10^{-5}$, $\epsilon_{tr}=10^{-6}$. In addition, for (a) the DIAG method was also used on a $8\times8$ lattice as indicated. In the simulation, 1000 MC steps were used for thermalizations and 1000 steps for measurements.

The results are in Fig. 14. Part (a) shows an excellent agreement among the several lattice sizes studied here. The abrupt change in the slope of the curve near $J_{AF}=0.15$ indicates a first-order transition, similar to that found in the one-orbital case and in previous literature. In (b), the full phase diagram is obtained. There are clear qualitative similarities with the results presented before by Aliaga *et al.* using a $4\times4$ cluster.[26] In particular, the curve defining the CE phase at low temperature has a positive slope rather than being vertical as in other cases. The fact that the TPEM gives results in

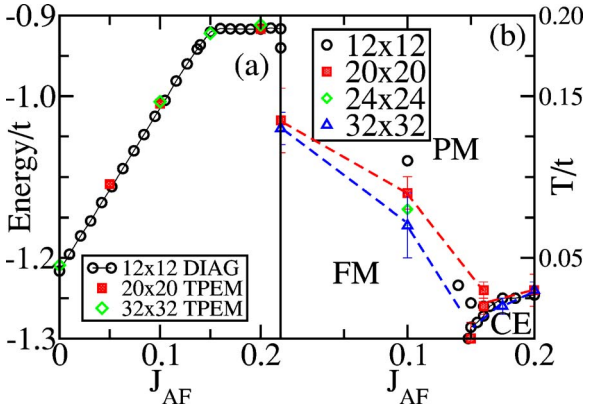


FIG. 14. (Color online) (a) Total energy vs $J_{AF}$ at low temperature ($T=0.01t$) for different lattices as indicated. For the $12\times12$ lattice the DIAG method was used, while for the others the TPEM was employed with $M=20$, $\epsilon_{pr}=10^{-5}$, $\epsilon_{tr}=10^{-6}$. In the simulation, 1000 MC steps were used for thermalizations and 1000 steps for measurements. (b) Phase diagram of Hamiltonian Eq. (8) varying temperature and $J_{AF}$ ($\lambda=0$). The three magnetically different regions: FM, PM, and CE are indicated. The phase diagram was calculated for different lattices as shown. For $12\times12$ the DIAG method was used and for the others the TPEM with $M=20$, $\epsilon_{pr}=10^{-5}$, $\epsilon_{tr}=10^{-6}$. The critical temperatures were obtained from the calculation of structure factors, as shown in Fig. 13.

TABLE II. CPU Times of the TPEM in seconds per five Monte Carlo steps for Hamiltonian Eq. (8) with $J_{AF}=0$ and inverse temperature $\beta=50$, and the lattices shown. The third column is the ratio of CPU time per lattice site. The computer used was an AMD Opteron(tm) 244, 1.8 GHz with 1 MB cache. The TPEM parameters were $M=20$, $\epsilon_{pr}=10^{-5}$, and $\epsilon_{tr}=10^{-6}$.

| $L\times L$ | CPU Time(s) | CPU Time/$N$ |
|---|---|---|
| $12\times 12$ | 122 | 0.85 |
| $20\times 20$ | 376 | 0.94 |
| $24\times 24$ | 564 | 0.98 |
| $32\times 32$ | 1063 | 1.04 |

good agreement with DIAG but on substantially larger systems is very encouraging and establishes this technique as a key method for a frontal attack to the CMR problem using realistic models and quenched disorder.

For completeness, CPU times for the case of the two-orbital model are provided in Table II. The CPU time per site does not change dramatically with $N$, close to the expected theoretical estimation for the TPEM. Clearly, lattices well beyond $32\times 32$ can be handled with this technique.

#### *2. Influence of phonons*

As explained in the introduction, the general scenario proposed for manganites does not depend on particular details of the competing phases, but in the competition itself and on the broad characteristics of these phases, such as their metallic and insulating properties.[6–8] Thus, to the extent that the FM metallic and CE insulating phases are found in competition, the particular value of the electron-phonon coupling λ is not of crucial relevance. The CE vs FM competition occurs approximately in the range of λ between 0 and 1 (beyond this number, the FM metallic phase transforms into a charge ordered insulator). We believe that λ is small in practice, since recent experiments are not finding evidence of a robust charge checkerboard. For example, see Ref. 64 for another estimation[67,68] of λ. In addition, theoretical studies have shown that a large λ renders the FM state also insulating.[26] Nevertheless, to confirm that the results are not severely affected by switching on λ, in Fig. 15 the phase diagram for $\lambda=0.5$ is presented on a lattice substantially larger than used in previous investigations.[26] Comparing Figs. 14 and 15, clearly both cases lead to very similar phase diagrams. Since removing the phononic degree of freedom speeds up the simulations, these results suggest that the future effort in this context could focus in the $\lambda=0$ case and still expect to find realistic conclusions. However, note that this issue is still controversial, namely, the experimental existence of a FM metallic phase in the phase diagram points toward a small λ, but there are several indications of a substantial Jahn-Teller effect in the insulator, which arises from a large λ effect.[7,27,65] Further theoretical and experimental work is needed to clarify this aspect.

### D. Density of states

As in the case of the one-orbital model, we also tested whether the TPEM technique can reproduce the DOS of the two-orbital model in the regime where the system is insulating (CE phase). The results are in Fig. 16. Part (a) shows a comparison between DIAG and TPEM on a $12\times 12$ cluster. The agreement is excellent for the case of $M=100$ (shown), and fairly acceptable for smaller values of $M$. For larger lattices that can only be studied with TPEM [part (b)], the results are also in good agreement with expectations. Then, no problems have been detected in calculating the DOS using the TPEM technique in the regime where the model is in an insulating state.

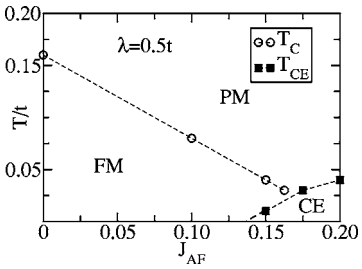


FIG. 15. Phase diagram of Hamiltonian (8) varying temperature and $J_{AF}$ for $\lambda=0.5$ and the harmonic parameters discussed in the text, i.e., with the inclusion of phonons. The critical temperatures were obtained from the calculation of structure factors on a $12\times 12$ lattice with the DIAG method. Note the similarity of this phase diagram with the result obtained at $\lambda=0.0$, suggesting that to simulate the competition between FM metallic and CE insulating regimes the presence of a robust electron-phonon coupling is not necessary.

### E. Conductances: Comparison TPEM vs DIAG, and results for increasing lattice sizes

As in the case of the one-orbital model, the final test for the two-orbital case is the calculation of the conductance. Results are shown in Fig. 17. Even using clusters much

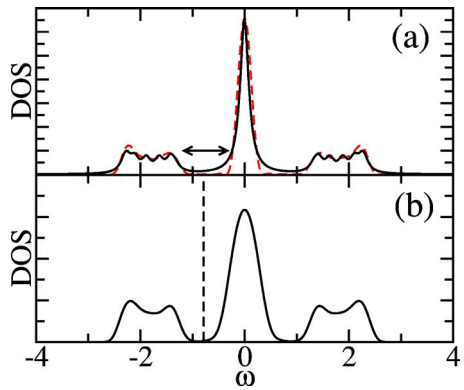


FIG. 16. (Color online) (a) DOS of a perfect CE phase (single spin configuration) obtained on a $12\times 12$ lattice calculated with the DIAG method (solid black line) and with the TPEM (dashed red line) using $M=100$. The chemical potential lies in the left gap (arrows) indicating that the system is an insulator. (b) DOS of the system with $J_{AF}=0.2$ (CE-phase ground state) on a $20\times 20$ lattice calculated with the TPEM using $M=100$, as described in the text. The location of the chemical potential is indicated by the vertical dashed line.

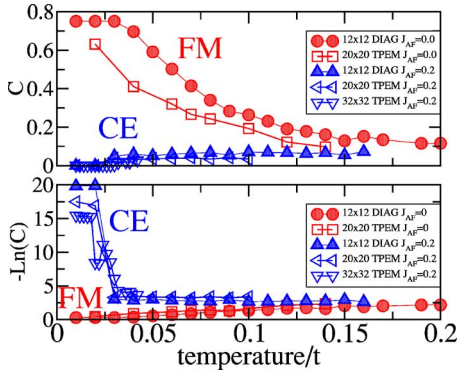


FIG. 17. (Color online) Upper panel: Conductance vs temperature for $J_{AF}=0.0$ (ferromagnet) and $J_{AF}=0.2$ (CE phase), different lattices sizes and algorithms, as indicated. Lower panel: Logarithm of the resistivity vs temperature for the same parameters as before.

larger than can be handled with DIAG, the behavior of the conductance is properly captured by TPEM. There are no hidden subtleties involved in this estimation of transport properties, opening the way toward many future applications of this technique.

### F. Influence of magnetic fields in the clean limit

Similarly as for the case of the one-orbital model, we have also studied the influence of a magnetic field in the case of the two-orbital model. The value of $J_{AF}$ was chosen to be 0.175, namely, on the CE side but close to the first-order metal-insulator transition. As shown in Fig. 18, the application of a relatively small field—in the natural units of the problem—leads to a drastic change in the resistivity at low temperatures. In this regime, the insulator is transformed into a metal (negative magnetoresistance). As remarked before, this is in agreement with previous studies carried out by Aliaga *et al.*,[26] showing that the "low temperature" large

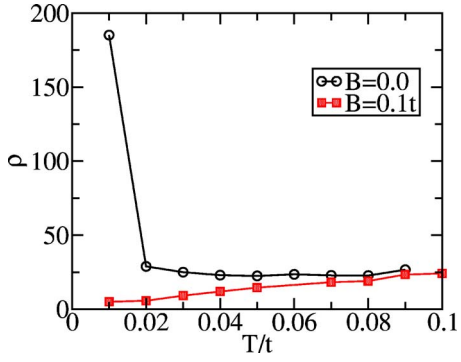


FIG. 18. (Color online) Effect of a small magnetic field on the resistivity of the CE phase, for couplings in the vicinity of the first order transition metal insulator. Shown is the resistivity vs $T$ at $J_{AF}=0.175$, $\lambda=0$, on a $20\times20$ lattice for $B=0.1t$ and without field ($B=0$) for comparison. Note the large change in the resistivity at low temperature, compatible with a colossal magnetoresistance. The TPEM was used with $M=30$, $\epsilon_{pr}=10^{-5}$, and $\epsilon_{tr}=10^{-6}$. 1,000 Monte Carlo steps were done for thermalization and an additional 100 more for measurements.

magnetoresistance materials[53] can be understood by double-exchange models in the clean limit. However, as in the case of one-orbital models studied before, the finite-temperature CMR effect in Mn oxides cannot be understood with clean limit models, as shown in Fig. 18, since the zero magnetic-field resistivity does not have the large peak characteristic of manganites. Future work with TPEM will address this issue including quenched disorder.

## V. CONCLUSIONS

In this paper, it has been shown that the computationally intensive exact-diagonalization algorithm for the study of CMR-manganite models can in practice be replaced by the truncated polynomial expansion method (TPEM) without any substantial loss in accuracy. The DIAG, although being exact, does not permit simulations of large clusters owing to the fact that the computational cost grows with the $4^{th}$ power of the system size $N$. On the other hand, the TPEM algorithm reduces the computational complexity to $O(N)$, thereby allowing for simulations of larger systems.

For both the one- and two-orbital double exchange model with interacting Mn spins, we have compared systematically the results calculated with both the diagonalization method and the TPEM algorithm. As the spin-spin coupling $J_{AF}$ is varied, the one-orbital model reveals a low-temperature first-order phase transition between conducting FM and insulating flux states in the vicinity of $J_{AF}=0.045$. For two orbitals, a similar first-order transition separates FM metallic and CE insulating phases. Our calculations presented here included a systematic study of the performance of the TPEM algorithm varying its parameters $M$, $\epsilon_{pr}$, and $\epsilon_{tr}$, already defined in the introductory sections. It was shown that the results of the TPEM algorithm converge to those of the DIAG algorithm with increasing $M$, and for $M\geq30$ TPEM results are sufficiently accurate to obtain phase diagrams with small error bars. This number appears to be fairly stable under changes in the model, couplings, and for different phases, and lattice sizes. Also nothing indicates that working at density different from 0.5, the focus of the current effort, will spoil the TPEM performance. (However, it is advisable to be particularly cautious near critical temperatures, where in some cases we found the need to increase $M$ to 40.) Similar systematic results were presented for the $\epsilon$'s. Overall, the general process of fixing TPEM parameters on small systems by comparing with DIAG and then using the same parameters on larger lattices appears reliable, and this method will be applied to other systems in the near future.

Parallelization of the TPEM algorithm makes it possible to study large clusters. Taking advantage of this possibility, in the absence of quenched disorder, we have made calculations on lattices of up to $40\times40$ sites even for the case of a finite Hund coupling in the one-orbital model. But previous calculations in the limit of $J_H=\infty$ used up to 8000 sites,[66] thus even accounting for the factors of 2 involved in comparing finite and infinite $J_H$ there is still room for further improvement. We have also checked that calculations of conductances, crucial to predict transport properties, also can be carried out smoothly with the TPEM, and in addition the size

effects are in general small. While obviously the increase in lattice size allows for more accurate determinations of critical temperatures, even more importantly these large lattices will be crucial for the next big step in large-scale manganite simulations which is the introduction of quenched disorder. This disorder is expected to lead to a percolativelike picture that causes the CMR phenomenon. Any percolative effect requires large systems, and having access to clusters substantially larger than those studied with DIAG is a key necessary condition to unveil the conceptual reason behind the CMR phenomenon.

Interesting physical results were also here reported. This includes the one-orbital phase diagram with a metal-insulator transition. But the main result in this context is the presence of an enormous magnetoresistance effect at low temperatures, even in the clean limit studied here. This effect was already anticipated by Aliaga *et al.* in their pioneering work on this subject on small systems.[26] The survival of the effect on the large clusters reachable by the TPEM, as described in this manuscript, shows that some forms of CMR found experimentally can already be accurately reproduced using realistic models, providing further support that a theoretical solution of the CMR puzzle is within reach. But for the most common form of CMR in Mn oxides at temperatures close to the Curie temperature, studies with quenched disorder will likely be needed.

Summarizing, we here reported a successful implementation of the TPEM for the study of double-exchange-like models for manganites. The technique has a CPU time that grows linearly with the number of sites, and in addition it is parallelizable. Thus, the main result is that a technique has been identified and tested that can contribute to a frontal attack of the most interesting problem in manganites: the analysis of large magnetoresistance effects in the presence of quenched disorder, when phases compete via a first-order transition in the clean limit. This "holy grail" of simulations will be the focus of our effort in the near future. It will demand at least an order of magnitude more effort than in the present manuscript, but this can be alleviated by increasing the number of nodes available for the simulations and we are already working on this aspect. The large-scale computational facilities at Oak Ridge National Laboratory will play a key role in reaching this ambitious goal.

## ACKNOWLEDGMENTS

Most of the computational work in this effort was performed at the supercomputing facilities of the National Center for Computational Sciences at the Oak Ridge National Laboratory (ORNL), managed by UT-Battelle, LLC, for the U.S. Department of Energy under Contract No. DE-AC05-000R22725. This work is supported by the LDRD program at ORNL and by the NSF Grant No. DMR-0443144. G.A. is supported by the Eugene P. Wigner Program at ORNL. We also acknowledge the help of J. A. Vergés in the study of conductances. This research used the SPF computer program and software toolkit developed at ORNL (http://mri-fre.ornl.gov/spf).

[1] *Colossal Magnetoresistance, Charge Ordering, and Related Properties of Manganese Oxides*, edited by C. N. R. Rao and B. Raveau, (World Scientific, Singapore, 1998).
[2] A. Moreo, S. Yunoki, and E. Dagotto, Science **283**, 2034 (1999).
[3] M. B. Salamon and M. Jaime, Rev. Mod. Phys. **73**, 583 (2001).
[4] N. Mathur and P. Littlewood, Phys. Today **January**, 25 (2003).
[5] K. H. Ahn, T. Lookman, and A. R. Bishop, Nature (London) **428**, 401 (2004).
[6] E. Dagotto, T. Hotta, and A. Moreo, Phys. Rep. **344**, 1 (2001).
[7] *Nanoscale Phase Separation and Colossal Magnetoresistance*, edited by E. Dagotto, (Springer Verlag, Berlin, 2002).
[8] E. Dagotto, New J. Phys. **7**, 67 (2005).
[9] E. Dagotto, Science **309**, 258 (2005).
[10] S. Yunoki and A. Moreo, Phys. Rev. B **58**, 6403 (1998).
[11] S. Yunoki, J. Hu, A. L. Malvezzi, A. Moreo, N. Furukawa, and E. Dagotto, Phys. Rev. Lett. **80**, 845 (1998).
[12] S. Yunoki, A. Moreo, and E. Dagotto, Phys. Rev. Lett. **81**, 5612 (1998).
[13] M. Y. Kagan, D. I. Khomskii, and M. V. Mostovoy, Eur. Phys. J. B **12**, 217 (1999).
[14] D. P. Arovas and F. Guinea, Phys. Rev. B **58**, 9150 (1998).
[15] A. Moreo, S. Yunoki, and E. Dagotto, Phys. Rev. Lett. **83**, 2773 (1999).
[16] T. Hotta, A. L. Malvezzi, and E. Dagotto, Phys. Rev. B **62**, 9432 (2000).
[17] V. J. Emery, S. A. Kivelson, and H. Q. Lin, Phys. Rev. Lett. **64**, 475 (1990).
[18] M. R. Ibarra and J. M. D. Teresa, Mater. Sci. Forum **302-303**, 125 (1999).
[19] M. Uehara, S. Mori, C. H. Chen, and S.-W. Cheong, Nature (London) **399**, 560 (1999).
[20] F. Parisi, P. Levy, L. Ghivelder, G. Polla, and D. Vega, Phys. Rev. B **63**, 144419 (2001).
[21] D. Louca, T. Egami, E. L. Brosha, H. Roder, and A. R. Bishop, Phys. Rev. B **56**, R8475 (1997).
[22] A. Moreo, M. Mayr, A. Feiguin, S. Yunoki, and E. Dagotto, Phys. Rev. Lett. **84**, 5568 (2000).
[23] Y. Imry and S. K. Ma, Phys. Rev. Lett. **35**, 1399 (1975).
[24] Y. Motome, N. Furukawa, and N. Nagaosa, Phys. Rev. Lett. **91**, 167204 (2003).
[25] C. Sen, G. Alvarez, and E. Dagotto, Phys. Rev. B **70**, 064428 (2004).
[26] H. Aliaga, D. Magnoux, A. Moreo, D. Poilblanc, S. Yunoki, and E. Dagotto, Phys. Rev. B **68**, 104405 (2003).
[27] A. J. Millis, B. I. Shraiman, and R. Mueller, Phys. Rev. Lett. **77**, 175 (1996).
[28] D. Akahoshi, M. Uchida, Y. Tomioka, T. Arima, Y. Matsui, and Y. Tokura, Phys. Rev. Lett. **90**, 177203 (2003).
[29] Y. Tomioka and Y. Tokura, Phys. Rev. B **70**, 014432 (2004).
[30] T. Nakajima, H. Kageyama, H. Yoshizawa, and Y. Ueda, J. Phys. Soc. Jpn. **71**, 2843 (2002).
[31] J. Burgy, M. Mayr, V. Martin-Mayor, A. Moreo, and E. Dagotto,

Phys. Rev. Lett. **87**, 277202 (2001).
[32] J. Burgy, A. Moreo, and E. Dagotto, Phys. Rev. Lett. **92**, 097202 (2004).
[33] Y. Motome and N. Furukawa, J. Phys. Soc. Jpn. **68**, 3853 (1999).
[34] N. Furukawa, Y. Motome, and H. Nakata, Comput. Phys. Commun. **142**, 410 (2001).
[35] N. Furukawa and Y. Motome, J. Phys. Soc. Jpn. **73**, 1482 (2004).
[36] Y. Motome and N. Furukawa, Phys. Rev. B **68**, 144432 (2003).
[37] G. Alvarez, C. Sen, N. Furukawa, Y. Motome, and E. Dagotto, Comput. Phys. Commun. **168**, 32 (2005).
[38] J. L. Alonso, L. A. Fernández, F. Guinea, V. Laliena, and V. Martín-Mayo, Nucl. Phys. B **596**, 587 (2001).
[39] J. L. Alonso, J. A. Capitan, L. A. Fernández, F. Guinea, and V. Martín-Mayor, Phys. Rev. B **64**, 054408 (2001).
[40] J. L. Alonso, L. A. Fernández, F. Guinea, V. Laliena, and V. Martín-Mayor, Phys. Rev. B **66**, 104430 (2002).
[41] S. Kumar and P. Majumdar, Phys. Rev. Lett. **92**, 126602 (2004).
[42] Y. Wang, G. M. Stocks, W. A. Shelton, D. M. C. Nicholson, Z. Szotek, and W. M. Temmerman, Phys. Rev. Lett. **75**, 2867 (1995).
[43] X. P. Li, R. W. Nunes, and D. Vanderbilt, Phys. Rev. B **47**, 10891 (1993).
[44] E. Hernandez and M. J. Gillan, Phys. Rev. B **51**, 10157 (1995).
[45] F. Mauri, G. Galli, and R. Car, Phys. Rev. B **47**, 9973 (1993).
[46] P. Ordejon, D. A. Drabold, M. P. Grumbach, and R. M. Martin, Phys. Rev. B **48**, 14646 (1993).
[47] E. B. Stechel, A. R. Williams, and P. J. Feilbelman, Phys. Rev. B **49**, 10088 (1994).
[48] P. Ordejon, E. Artacho, and J. M. Soler, Phys. Rev. B **53**, R10441 (1996).
[49] R. Car and M. Parrinello, Phys. Rev. Lett. **55**, 2471 (1985).
[50] S. Goedecker and L. Colombo, Phys. Rev. Lett. **73**, 122 (1994).
[51] W. Kohn, Phys. Rev. Lett. **76**, 3168 (1996).
[52] S. Goedecker and L. Colombo, Rev. Mod. Phys. **71**, 1085 (1999).
[53] Y. Tokura, H. Kuwahara, Y. Moritomo, Y. Tomioka, and A. Asamitsu, Phys. Rev. Lett. **76**, 3184 (1996).
[54] R. N. Silver and H. Röder, Phys. Rev. E **56**, 4822 (1997).
[55] A. Weisse, G. Wellein, A. Alvermann, and H. Fehske, Rev. Mod. Phys. **78**, 275 (2006).
[56] M. Yamanaka, W. Koshibae, and S. Maekawa, Phys. Rev. Lett. **81**, 5604 (1998).
[57] D. F. Agterberg and S. Yunoki, Phys. Rev. B **62**, 13816 (2000).
[58] E. O. Wollan and W. C. Koehler, Phys. Rev. **100**, 545 (1955).
[59] *Field-Theory, the Renormalization Group and Critical Phenomena*, edited by D. Amit and V. Martin-Mayor, (World Scientific, Singapore, 2005).
[60] L.-W. Wang and A. Zunger, Phys. Rev. Lett. **73**, 1039 (1994).
[61] G. Alvarez and T. C. Schulthess, Phys. Rev. B **73**, 035117 (2006).
[62] R. N. Silver, H. Roeder, A. F. Voter, and J. D. Kress, J. Comput. Phys. **124**, 115 (1996).
[63] J. A. Vergés, Comput. Phys. Commun. **118**, 71 (1999).
[64] G. Subias, J. Garcia, J. Blasco, M. Grazia Proietti, H. Renevier, and M. Concepcion Sanchez, Phys. Rev. Lett. **93**, 156408 (2004).
[65] H. Röder, J. Zang, and A. R. Bishop, Phys. Rev. Lett. **76**, 1356 (1996).
[66] Y. Motome and F. Furukawa, J. Phys. Soc. Jpn. **72**, 2126 (2003).
[67] Y. Tokura, *Colossal Magnetoresistive Oxides* (Gordon and Breach, New York, 2000).
[68] Photoemission experiments estimate the value of the dimensionless Jahn-Teller coupling $\lambda$ in the range 1–1.6, D. S. Dessau and Z-X. Shen, Colossal Magnetoresistance Oxides in Ref. 67.